Journal of The
Electrochemical Society

OPEN ACCESS

Analysis of Battery-like and Pseudocapacitive Ion Intercalation Kinetics via Distribution of Relaxation Times

To cite this article: Yoga Trianzar Malik *et al* 2024 *J. Electrochem. Soc.* **171** 110515

Journal of The Electrochemical Society, 2024 **171** 110515

Analysis of Battery-like and Pseudocapacitive Ion Intercalation Kinetics via Distribution of Relaxation Times

Yoga Trianzar Malik,[1,2] Michael Braig,[1,2,3] Patrice Simon,[4,5] Roswitha Zeis,[1,2,3,6] and Simon Fleischmann[1,2,*,z]

[1]*Helmholtz Institute Ulm (HIU), 89081 Ulm, Germany*
[2]*Karlsruhe Institute of Technology (KIT), 76021 Karlsruhe, Germany*
[3]*Faculty of Engineering, Department of Electrical Engineering, Friedrich-Alexander-Universität Erlangen-Nürnberg (FAU), 91058 Erlangen, Germany*
[4]*Université Toulouse III Paul Sabatier, CIRIMAT, UMR-CNRS 5085, 31062 Toulouse, France*
[5]*Réseau sur le Stockage Electrochimique de l´Energie (RS2E), Fédération de Recherche, CNRS 3459, Amiens 80039, France*
[6]*Faculty of Applied Science & Engineering, Department of Mechanical & Industrial Engineering, University of Toronto, Toronto, Ontario, M5S 3G8, Canada*

Improving the kinetics of electrochemical ion intercalation processes is of interest for realizing high-power electrochemical energy storage. This includes classical battery-like intercalation and pseudocapacitive intercalation processes with a capacitor-like electrochemical signature. Electrochemical methods are needed to probe the kinetics of such complex multistep processes in detail. Here, we present the use of the distribution of relaxation times (DRT) analysis of electrochemical impedance data to identify the kinetic limits of intercalation reactions. We study the lithium intercalation reaction in TiS_2 from organic and aqueous electrolytes as a model system. The material can exhibit both battery-like and pseudocapacitive intercalation regimes depending on the potential range, variable diffusion lengths by adjusting its particle size, and a tunable degree of solvent cointercalation by choosing the electrolyte solvent. Using DRT, we can distinguish between the kinetic limitations imposed by solid-state ion diffusion, interfacial ion adsorption and transport, and ion desolvation processes. Thus, DRT analysis can complement existing methods, such as voltammetry or 3D-Bode analysis, to better understand the kinetics of intercalation reactions.

 [DOI: 10.1149/1945-7111/ad8d51]

Manuscript submitted September 23, 2024; revised manuscript received October 25, 2024. Published November 19, 2024.

Supplementary material for this article is available online

Ion intercalation reactions within layered or two-dimensional host materials have attracted considerable attention in the field of electrochemical energy storage. They involve the insertion of ions into the interlayer spaces of host materials causing small structural changes. This yields relatively high chemical and electrochemical reversibility and cycling stability,[1] making layered materials promising candidates for applications in high-power energy storage devices. Currently, improving the kinetics of ion intercalation reactions is at the core of such research efforts. This includes a wide variety of approaches, including reducing crystallite sizes,[2,3] carbon nanocomposite formation,[4,5] expanding interlayer distances,[6,7] electrode architecture design with hierarchical porosity,[8,9] or facilitating ion-solvent cointercalation reactions.[10–12] While any of these strategies can enhance the overall kinetics, they typically aim to overcome different limitations of the charge storage process.

The ion intercalation process is comprised of several distinct steps, each occurring at different time scales. These steps include ion transport through the electrolyte towards the electrochemical interface, ion desolvation, ion surface transport to the insertion site, ion transport through a passivating layer, electron transfer, and solid-state ion diffusion.[12–15] Deconvoluting the contribution of individual steps to the overall electrochemical kinetics is critical. It allows to elucidate how specific sub-steps of the intercalation process are affected by modifying individual components of the electrochemical system (e.g., electrode material structure, electrode architecture, electrolyte composition, etc.).

Such deconvolution efforts are further complicated by the possibility of simultaneously occurring charge storage mechanisms in an electrochemical system. In addition to battery-like intercalation processes characterized by clear redox peaks in the cyclic voltammogram (CV), capacitor-like processes such as double-layer capacitance and/or pseudocapacitance with rectangular CV signatures can be present. Intercalation pseudocapacitance typically arises from solid-solution intercalation reactions in absence of phase transformations and with only minimal volumetric changes of the host material, leading to surface-limited kinetics at elevated charging/discharging rates.[16–18] They can also be caused by reduced ion-host interaction, especially when ion-solvent cointercalation takes place.[19]

Electrode kinetics are often analyzed by voltammetry, leveraging the sweep rate (ν) dependence of redox peak currents (i) according to

$$i = a\nu^b, \quad [1]$$

where a and b are adjustable parameters. For ideal semi-infinite diffusion-controlled charge storage processes, b = 0.5, whereas ideal surface-limited processes exhibit b = 1 ("b-value analysis").[20] However, assigning kinetics according to this b-value suffers from redox peak shifts/broadening and ohmic drops, especially at higher currents.[21] It is also prone to misinterpretation, often leading to mistakenly labeling "fast" battery materials as (pseudo)capacitive,[22,23] which is typically encountered when finite-length diffusion leads to b-values between 0.5 and 1.[18]

More reliable analysis of electrode kinetics is enabled by electrochemical impedance spectroscopy (EIS), which probes electrochemical processes including ion intercalation kinetics over wide time scales.[24,25] The resulting Nyquist plots (imaginary vs real impedance) can be interpreted using electrical equivalent circuits. However, fitting the experimental data is non-trivial, and the use of physical models requires deep prior knowledge of the system.[24] Three-dimensional Bode plot representations of impedance spectra (phase angle/real capacitance vs frequency vs electrode potential) have recently been presented for direct visualization of charge storage kinetics,[26–28] providing the possibility to distinguish double-layer, pseudocapacitive, and battery-like processes. However, this method utilizes an electrical equivalent circuit of a resistor and a capacitor in series,[29]

*Electrochemical Society Member.
[z]E-mail: simon.fleischmann@kit.edu

which is an oversimplification if the entire complexity of a multi-step intercalation processes is investigated.

The distribution of relaxation times (DRT) method provides an alternative way to interpret EIS data. Thereby, the impedance data are analyzed by a continuous distribution of RC-elements in the space of relaxation times.[30] The advantage of this method is that no a priori choice of equivalent circuit has to be made (it is assumption-free). Thus, distinct steps of charge storage processes can be separated according to their specific time constant.[31] The resulting DRT function shows peaks representing the resistance of each individual sub-steps of complex electrochemical processes.[30–33]

To validate its applicability in a typical high-power electrochemical intercalation-based charge storage process, herein, the kinetics of the lithium intercalation reaction in TiS_2 is studied by DRT analysis. TiS_2 was the first host material for electrochemical lithium intercalation described by Prof. Whittingham[34] and it exhibits a unique lithiation mechanism from organic electrolytes which is characterized by a diffusion-limited, battery-like region (in the Li_xTiS_2 range of $0 < x < 0.5$), and a surface-limited, pseudocapacitive region (in the Li_xTiS_2 range of $0.5 < x < 1$).[35,36] Moreover, when utilizing electrolytes based on water or diglyme solvent, ion-solvent co-intercalation can be observed instead of bare ion intercalation from carbonate electrolytes.[37,38] Finally, the TiS_2 particle size can easily be modified via ball-milling,[39] allowing to change diffusion path lengths. These features make TiS_2 an ideal model system because several parameters can be modified individually by experimental design, and thus the resulting impedance response can be analyzed in detail.

Experimental Description

Materials.—Titanium disulfide (TiS_2) is purchased from Fischer Chemicals. 1 M lithium hexafluorophosphate ($LiPF_6$) in a mixture (50:50 vol%) of ethylene carbonate (EC) and dimethyl carbonate (DMC) is purchased from Solvionic. Lithium bis(trifluoromethane) sulfonimide (LiTFSI, 99%), carbon black (C65, CB), polyvinylidene fluoride (PVDF) and N,N-dimethyl pyrrolidone (NMP) are purchased from Sigma-Aldrich.

Preparation of TiS_2-based electrodes and electrochemical cells.—TiS_2 with reduced particle sizes (labelled nano-TiS_2) is prepared via ball-milling in a zirconia jar with a milling time of 8 h at 600 rpm. 9 large and 10 small zirconia balls are employed with a diameter of 10 mm and 0.1 mm, respectively, with a mass ratio of 31.5 g balls to 1 g sample.

The slurry consists of active material (pristine or nano-TiS_2), PVDF, and CB with ratio of 8:1:1. Pristine or nano-TiS_2 powders were grinded together with CB using a mortar and transferred into a small container together with 2 wt% PVDF in NMP solution and then transferred into a speed mixer (ARE-250, Thinky Mixer), where it was mixed at 2000 rpm for 10 min.

The resulting slurry was coated onto carbon-coated aluminum foil with a wet film thickness of 60 μm using a doctor blade and dried overnight in an oven at 80 °C. Electrodes with a diameter of 12 mm and an areal loading of ca. 1 mg cm^{-2} were cut using a handheld electrode puncher and pressed in a hydraulic press with 5 tons weight for 1 min. These electrodes were further dried under vacuum at 60 °C for 6 h in a glass tube (Büchi), in which they were transferred into an argon-filled glovebox (MBraun, H_2O and O_2 <0.1 ppm).

Swagelok-type 3-electrode cells ("T-cells") were assembled using TiS_2-based electrodes as working electrode and metallic lithium discs (Honjo, 12 mm diameter) as counter and reference electrodes. A glass microfiber filter (Whatman grade GF/D) with a diameter of 13 mm was used as separator and 120 μl of LP30 (1 M $LiPF_6$ in ethylene carbonate and dimethyl carbonate (EC/DMC) with 1:1 volumetric ratio) or 1 M LiTFSI in 2 G were used as electrolyte. Swagelok-type 3-electrode cells ("T-cells") were also used for impedance measurements, utilizing an additional piece of lithium metal as reference electrode.

Testing of TiS_2 in aqueous electrolyte was conducted in a custom-made three-electrode cell made of polyether ether ketone (PEEK), which is described in detail in Ref. 40. With the same PVDF binder and composition, the TiS_2 slurry was cast on titanium foil current collector (MHUI, 10 μm foil thickness) for use as working electrode. PTFE-bound activated carbon (YP-50 F, Kuraray) served as pseudo-reference electrode and an oversized PTFE-bound activated carbon electrode as the counter electrode in 1 M LiTFSI aqueous electrolyte.

Structural characterization.—Scanning electron microscopy (SEM) images were collected using a Gemini microscope with 5 kV acceleration voltage. Powder X-ray diffraction (XRD) was performed in Bragg-Brentano geometry using a Bruker D8 Advance diffractometer using a Cu Kα radiation (λ = 1.5406 Å) with a 0.02° step size with a dwell time of 1 s. Raman spectroscopy was performed using a Renishaw InVia confocal Raman microscope with a 532 nm excitation laser. The laser power was kept at 100 μW to prevent the degradation of samples. Three different spots were investigated to ensure the samples homogeneity. The particle size distribution was characterized using a laser diffraction particle size analyzer (Mastersizer 3000, Malvern) to measure the size of non-spherical particles via dynamic light scattering (DLS). A mixture of isopropanol and deionized water (1:1 volumetric ratio) was used as a dispersant, sonication was employed to ensure dispersion of the powder and to avoid agglomeration prior to the measurement.

Electrochemical analysis.—Cyclic voltammetry (CV) was performed at a sweep rate of 0.1 mV s^{-1} in a potential range of 3.0–1.5 V vs Li/Li^+. Galvanostatic charge/discharge (GCD) was performed at a constant current rate of 100 mA g^{-1} (with respect to active material) in the same potential window. Staircase potential-electrochemical impedance spectroscopy (SPEIS) was performed in 21 steps between 3 to 1.5 V vs Li/Li^+, corresponding to ca. 71 mV increments. Between each EIS measurement, a 10 min chronoamperometric step was performed to reach steady state conditions. The frequency range was set from 1 MHz to 10 mHz. Each frequency was averaged for 3 times, and 10 points per decade were recorded. All measurements were carried out in a temperature-controlled chamber (Binder) at 20 °C using Biologic potentiostats (VMP-3e and VMP-300).

Distribution of relaxation times analysis.—The distribution of relaxation times (DRT) analysis was conducted utilizing the Relaxis software (rhd Instruments). The quality of the used impedance data was assessed prior to DRT analysis via Kramers-Kronig transformation. The obtained residuals are generally below 1.5% with some outliers, indicating good data quality sufficient for DRT analysis (Fig. S1).

The recorded impedance spectra were transformed into a DRT function, restricting the data points to the frequency range of 500 kHz to 0.12 Hz. Interpreting impedance spectra proves challenging due to overlapping effects and nonideal processes. To facilitate this, the DRT method employs fitting impedance data with an infinite series of RC-elements alongside an ohmic resistance. Within the selected frequency range, each measurement exhibited data points demonstrating inductive behavior, necessitating the inclusion of an inductor in the model to ensure accuracy, particularly at higher frequencies.

Within the DRT function, each peak signifies a distinct physicochemical process, with the area under the peak indicating its corresponding resistance. The calculation of the DRT function, represented as g(f), poses an ill-posed mathematical problem, necessitating the careful selection of a regularization parameter (lambda) to derive meaningful results. An improperly chosen regularization parameter may induce oscillations, false peaks, or merge multiple processes into a singular peak. Thus, the selection of lambda is crucial for obtaining accurate and reliable outcomes.

Results and Discussion

Structural characterization.—In order to analyze the impact of diffusion path length on the electrochemical lithium intercalation properties in TiS_2, model materials of two distinct particle sizes are employed. Bulk-TiS_2 is commercially available and investigation of its morphology by scanning electron microscopy (SEM) reveals mainly flake-like particles with lateral sizes in the range of tens of micrometers (Fig. 1A). The particle size of bulk-TiS_2 is then reduced by ball-milling for 8 h.[39] The resulting particles with flake-like morphology show a reduced particle size, ranging from several hundreds of nanometers to a few micrometers (Fig. 1B).

The qualitative observations of particle size from SEM are quantitatively confirmed by dynamic light scattering (DLS), indicating a reduction in mean secondary particle diameter from approximately 30 to 5 μm (Fig. 1C). Argon sorption measurements reveal type III isotherms according to IUPAC classification[41] for both bulk- and nano-TiS_2, with negligible hysteresis loops between adsorption and desorption branches (Fig. 1D), revealing a nonporous or macroporous character for both materials. With the Brunauer–Emmett–Teller (BET) analysis a roughly doubled specific surface area is determined after ball-milling, increasing from ca. 12 to 24 $m^2\ g^{-1}$.

X-ray diffractograms of both materials indicate identical phases of trigonal 1T-TiS_2 (space group space group $P\bar{3}m1$), with no significant broadening of the (001) interlayer spacing signal for nano-TiS_2 (Fig. 1E). Furthermore, secondary phases were not observed. Raman spectroscopy shows typical signals of E_{1g}, A_{1g}, and S_h (Fig. 1F), further validating the absence of impurities in both samples.[42] Overall, the combination of structural characterization methods indicates that (1) no chemical changes occur and phase-pure TiS_2 is maintained after mechanical treatment, and (2) no significant/preferential exfoliation is caused by the mechanical treatment. This suggests that the main mode of particle size reduction during ball-milling is breaking of basal planes.

Baseline electrochemical characterization.—As a first step, the electrochemical lithium intercalation properties of bulk- and nano-TiS_2 are evaluated to establish a baseline for the subsequent, in-depth analysis by electrochemical impedance spectroscopy (EIS). In cyclic voltammograms (CVs) recorded at a low sweep rate of 0.1 mV s^{-1}, two regions can be identified in both materials. A battery-like region with a pair of distinct redox peaks is observed above ca. 2.25 V, and a capacitor-like region with rectangular current profile is found below ca. 2.25 V (Fig. 2A). This is consistent with previous literature reports on lithium intercalation into TiS_2 from carbonate-based electrolytes and was explained by the different intercalation-induced deformation behavior of TiS_2 in the two regimes.[35,36] The battery-like region is associated with volumetric expansion of the TiS_2 host upon lithiation with diffusion-limited kinetics, while the capacitor-like region exhibits no volumetric changes and surface-limited kinetics.[35,36] Previous studies reported these findings only for commercial bulk-TiS_2. Our results of highly similar CVs for both materials suggest that the same intercalation mechanism is also present in ball-milled nano-TiS_2. Galvanostatic charge/discharge profiles support this assumption by largely overlapping for both materials (Fig. 2B). The measured specific anodic/delithiation capacities at a rate of 100 mA g^{-1} are 192 and 215 mAh g^{-1} for bulk- and nano-TiS_2, respectively, close to the theoretical capacity of 239 mAh g^{-1} for the reversible (de)intercalation of 1 Li^+ per TiS_2.[35]

The kinetics of electrochemical intercalation reactions, specifically for high-power systems, are often analyzed using the so-called "b-value analysis," which aims to deconvolute kinetically diffusion-limited from surface-limited current contributions to the overall measured current.[20,23] The method takes advantage of the scan rate dependence of redox peak currents according to Eq. 1 given above. The technique is employed for bulk- and nano-TiS_2 for a series of cyclic voltammograms in a range of scan rates from 0.1–10 mV s^{-1} (Figs. 3A–3B). Extraction of the peak currents of cathodic (anodic) processes in both materials yields b-values of 0.76 (0.80) for bulk-TiS_2 and 0.85 (0.86) for nano-TiS_2 (Figs. 3C–3D). When probing the lithiation of bulk-TiS_2 from aqueous electrolyte, b-values of 0.66–0.67 are observed (Fig. S2).

A meaningful interpretation for the overall intercalation kinetics of such values between 0.5 and 1 is challenging, as they may point to finite-length diffusion effects (in contrast to semi-infinite diffusion, which should theoretically give $b = 0.5$). This makes them highly sensitive toward particle size, i.e., diffusion lengths.[18] Moreover, CVs recorded at faster scan rates show significant shifts of the redox potentials due to increasing overpotentials, ohmic contributions, and peak broadening, making the selection of individual "peak currents" more and more challenging and prone to mistakes. A more detailed description of the b-value analysis can be found in literature, also emphasizing the limitations of the method.[18,22,23,43] To gain more meaningful insights into the kinetics of each individual step of the intercalation process, it is necessary to employ EIS analysis.

Distribution of relaxation times analysis.—In the following, the kinetics of the electrochemical lithium intercalation process into TiS_2 are probed in detail by EIS and subsequent DRT analysis. The electrochemical system is varied in three controlled ways. First, the transition from battery-like to capacitor-like/pseudocapacitive intercalation is probed, leveraging the existence of both regions in TiS_2 at different potentials. Second, the influence of particle size (i.e., diffusion path length) is probed by investigating bulk- vs nano-TiS_2. Third, desolvated vs solvated ion intercalation (i.e., ion-solvent cointercalation[12]) is evaluated by comparing lithiation from carbonate-based vs diglyme- or water-based electrolytes. This enables us to identify and assess the impact of individual sub-steps of the intercalation process on the associated EIS/DRT response.

The DRT transformation of EIS data requires the selection of the regularization parameter λ. It determines the fit quality and lower regularization parameters generally lead to better fits. If λ is chosen too low, artificial peaks can be created, but if λ is chosen too high, merging of distinct peaks can mask individual processes resulting in a loss of information in the DRT transformation. This is demonstrated in Figs. S3A, S3C for the choice of various regularization parameters λ. This is why the sum of square residuals (SSR) is used as an indicator of sufficiently low λ, when the residual between measured and DRT-reconstructed EIS data no longer decreases.[32] In the present case, this leads to the selection of the λ value of 10^{-3}. The procedure is demonstrated for an exemplary impedance spectrum, its DRT transformation, the comparison of measured and reconstructed EIS from DRT, and the related SSR for various regularization parameters in Fig. 4. The impact of different λ values on the resulting DRT curves, as well as the impact of a shape factor[44] (0.38 chosen in this study), is further demonstrated in Fig. S3. Further, more detailed information on the choice of the regularization parameter has been the topic of previous works.[45–47]

EIS spectra are recorded at various states of charge, allowing to assess the impedance response at different stages of TiS_2 lithiation. All impedance spectra (in 21 increments between 3.0 and 1.5 V vs Li^+/Li) and the related DRT transformations are presented in Fig. S4. Generally, the obtained DRT profiles obtain six to seven signals, each corresponding to individual processes in the electrochemical system occurring at different time scales (as indicated by the frequency). Based on the general assumptions about impedance analysis of electrochemical intercalation reactions,[48–51] we first assign the DRT signals to certain sub-processes a priori and confirm this assignment subsequently by experimental modifications of the electrochemical system.

The lowest frequency process (P1) is assigned to the solid-state diffusion process of the intercalant within the TiS_2 host lattice.[35,48] Mid-frequency processes (P2–P4) are often summarized as charge transfer resistance, which in intercalation reactions encompasses both the electron transfer (from the current collector to the transition metal center of the active material) and ion transfer (from the electrolyte solution into the intercalation host) processes.[15] Generally, these charge transfer-related steps entail interfacial processes including surface adsorption of solvated ions, surface

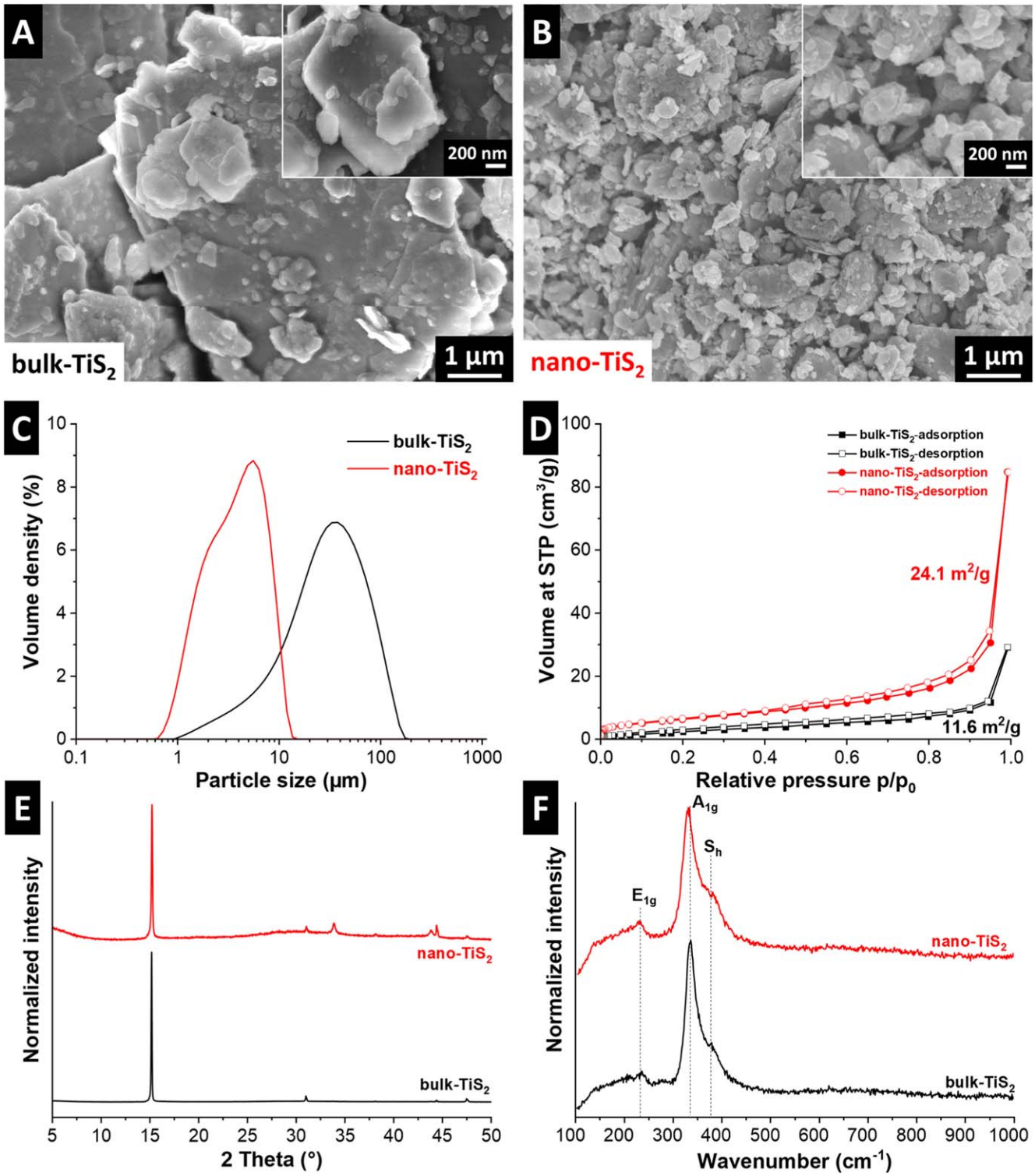

Figure 1. Structural characterization. Scanning electron micrographs of (A) bulk-TiS_2 and (B) ball-milled nano-TiS_2. Inset figures show larger magnification. (C) Dynamic light scattering, (D) argon sorption isotherms, (E) X-ray diffractograms, and (F) Raman spectra of bulk- and nano-TiS_2 samples.

transport to an insertion site and through a potential passivation layer, and desolvation of the ion prior to insertion (in the case of organic electrolytes).[15,52] It is noteworthy that there are only two DRT signals in the mid-frequency range when probing the pseudocapacitive potential region, regardless of particle size, whereas three signals are observed in the battery-like potential region. We hypothesize that this is related to the availability of different insertion sites in the pseudocapacitive intercalation region due to the increased d-spacing, as predicted in previous work,[53] therefore reducing impedance posed by surface transport. Three high frequency signals (P5–P7) are related to ohmic resistances of the electrochemical cell components (electrolyte and contact resistances) as well as impedance contribution of the reference electrode, which do not strongly vary across the different samples and potential regions. Thus, they are subsequently excluded from the discussion as they contain little information on the intercalation process itself.

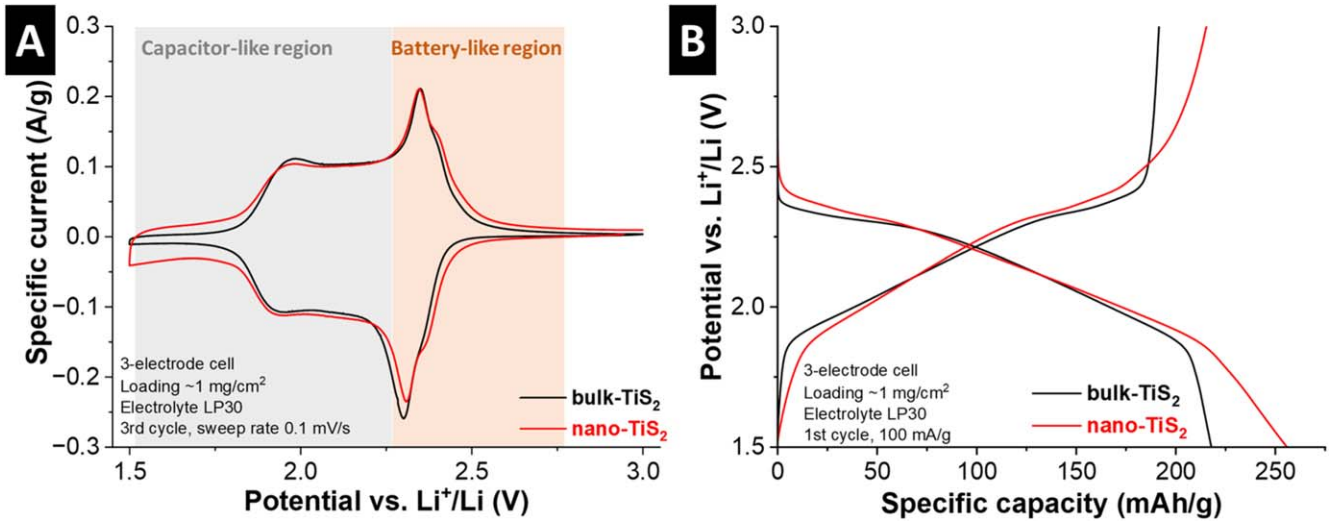

Figure 2. Electrochemical characterization of bulk- and nano-TiS_2. (A) Cyclic voltammograms recorded at a sweep rate of 0.1 mV s^{-1}. (B) Galvanostatic charge/discharge profiles at a specific current of 100 mA g^{-1}. All experiments are conducted in 3-electrode cells ("T-cells") with lithium metal counter and pseudo-reference electrodes in LP30 electrolyte at a constant temperature of 20 °C.

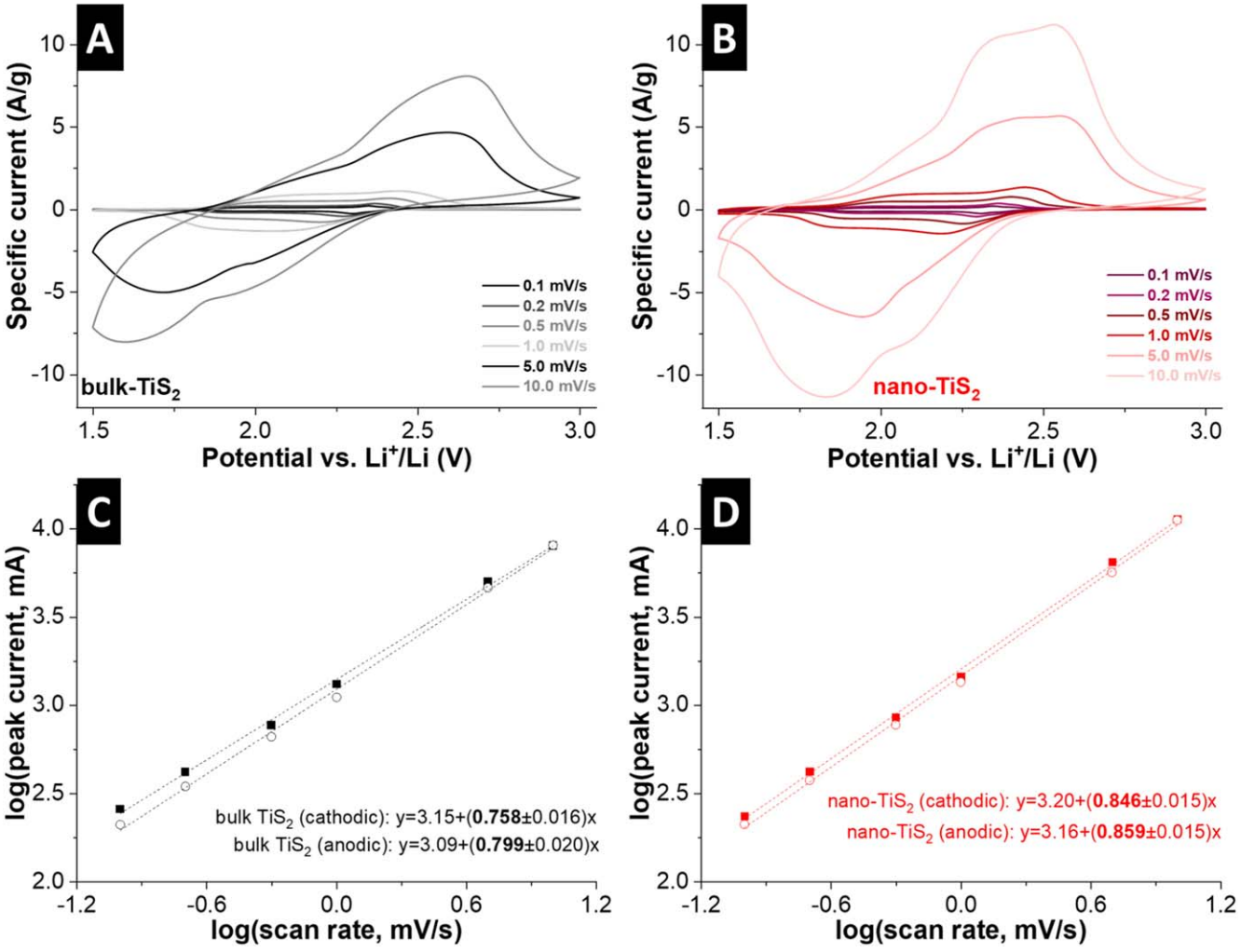

Figure 3. Kinetic analysis by b-value analysis. Cyclic voltammograms at sweep rates from 0.1–10 mV s^{-1} of (A) bulk-TiS_2 and (B) nano-TiS_2. Corresponding b-value analysis with anodic and cathodic peak currents at various sweep rates of (C) bulk-TiS_2 and (D) nano-TiS_2. The slopes of the linear fit equations indicate the "b-value" of the corresponding process.

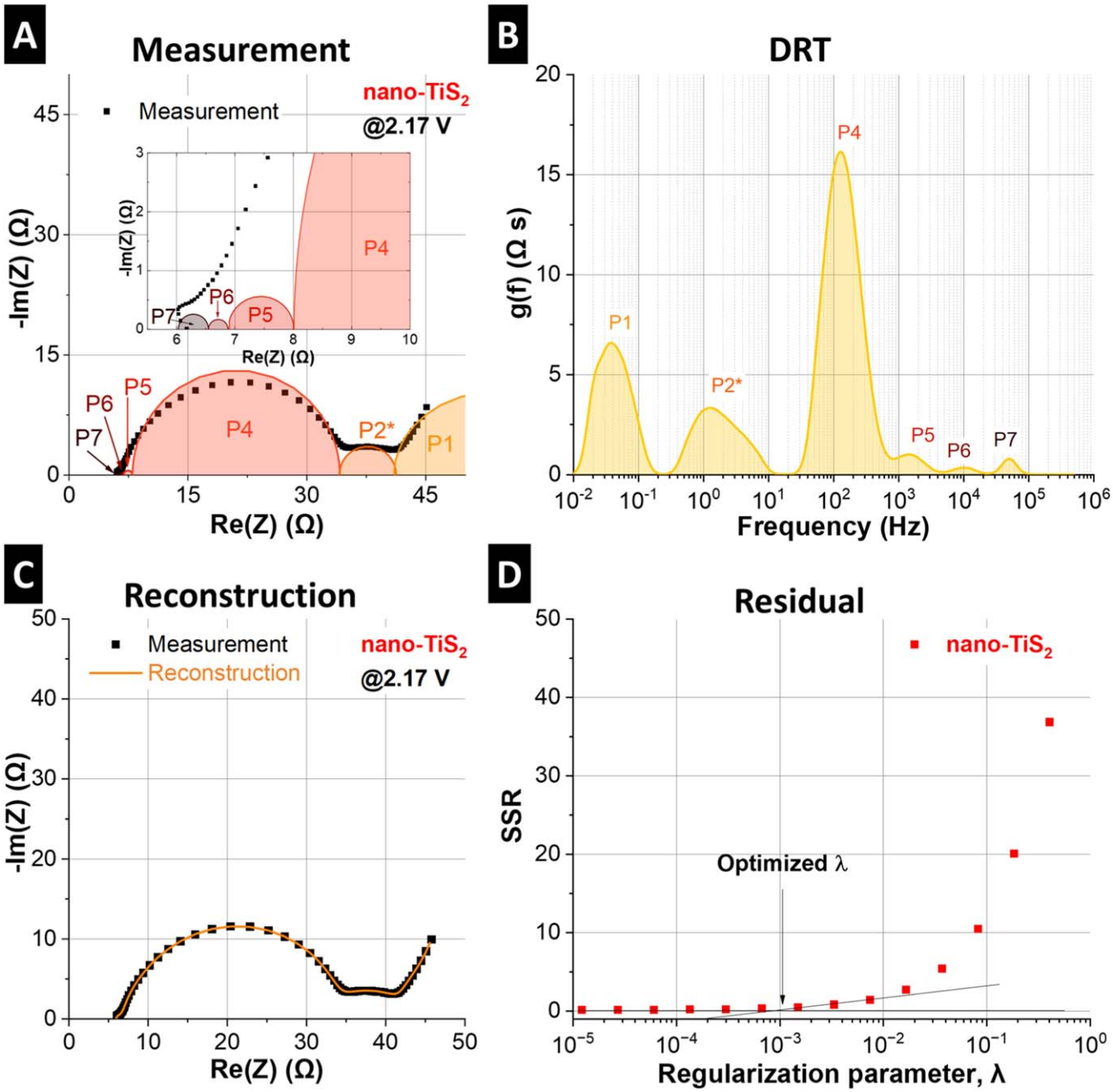

Figure 4. DRT analysis of representative Nyquist-plot. (A) Exemplary Nyquist plot with indicated processes extracted from DRT, and (B) the derived DRT plot using regularization parameter 10^{-3}. (C) Reconstruction of Nyquist plot from DRT, (D) related sum of square residuals (SSR) as a function of regularization parameters.

For analyzing the kinetics of the battery-like and pseudocapacitive Li^+ intercalation regions in TiS_2, impedance spectra are recorded at 2.40 V and 2.17 V vs Li^+/Li, respectively. A comparison of the impedance signals for the bulk-TiS_2 electrode is shown in Fig. 5A. The Nyquist plots exhibit pronounced semi-circles in the mid-frequency region, followed by Warburg-type behavior in the low frequency region. A change for both features in the Nyquist plots is visible from battery-like to pseudocapacitive regions. The slope in the Warburg region is higher in the pseudocapacitive region, which is indicative of reduced solid-state ion diffusion limitations. Moreover, the magnitude of the mid-frequency semi-circle is reduced in the pseudocapacitive region, indicative of a reduced charge transfer resistance. However, the underlying contributions to the charge transfer resistance remain unclear from the Nyquist plot, which is why DRT is employed to analyze the transition from battery-like to pseudocapacitive behavior in more detail.

First, a strong reduction in the DRT signal related to solid-state diffusion of Li^+ within the TiS_2 lattice (P1) in the low frequency range is observed when transitioning to the pseudocapacitive potential region (Fig. 5B), which is consistent with the general assumption about non-diffusion limited behavior of pseudocapacitive charge storage phenomena[17,18] and with previous reports on reduced diffusion limitation in TiS_2 in this potential region.[35,36] It is also consistent with the higher slope observed in the Warburg region of the Nyquist plot (Fig. 5A). In the mid-frequency range, DRT signals related to interfacial ion adsorption and transport also strongly decrease in the pseudocapacitive region, with the intensity of P2 and P3 strongly reducing, resulting in P2* (Fig. 5B). However, the DRT signal we assign to ion desolvation (P4) increases in intensity in the pseudocapacitive region, including contributions from P3 from the battery-like region (Fig. 5B). This behavior is in

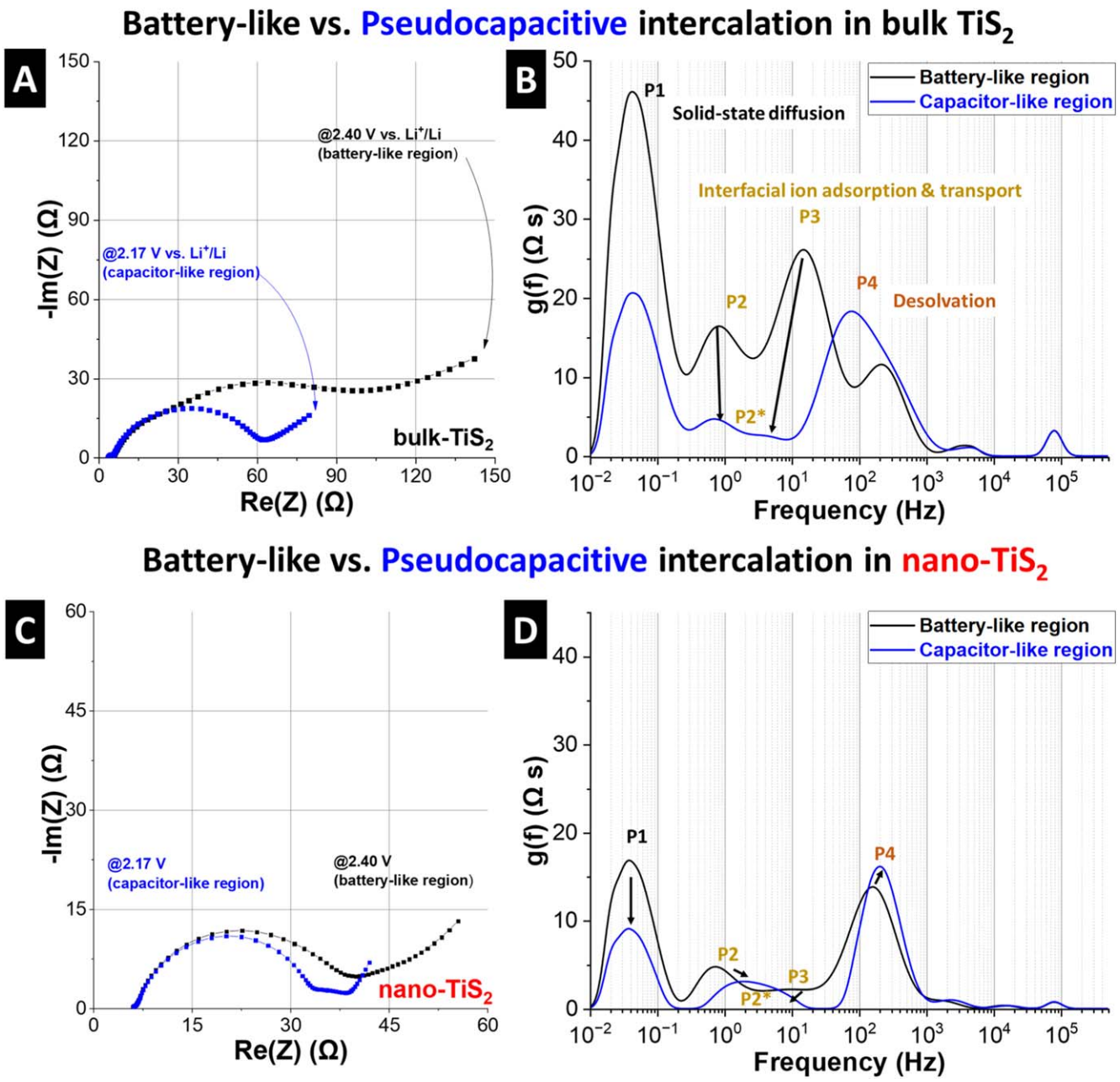

Figure 5. Battery-like vs pseudocapacitive intercalation in bulk-TiS_2 and nano-TiS_2. (A) Nyquist plots of bulk-TiS_2 from EIS measurements at 2.4 V (battery-like region) and at 2.17 V vs Li^+/Li (capacitor-like or pseudocapacitive region) and (B) related DRT transformation of both Nyquist plots. (C) Nyquist plots of nano-TiS_2 from EIS measurements at 2.4 V (battery-like region) and at 2.17 V vs Li^+/Li (capacitor-like or pseudocapacitive region) and (D) related DRT transformation of both Nyquist plots.

line with experimentally measured solvent accumulation at the interface in the pseudocapacitive region.[36] Consequently, when transitioning from battery-like to pseudocapacitive lithiation in bulk-TiS_2, kinetic limitations of solid-state diffusion and surface adsorption diminish, while ion desolvation now poses a more severe impedance to the charge storage process. This nuanced behavior is not easily visible from the Nyquist plots alone.

Next, the impedance of nano-TiS_2 in the battery-like and pseudocapacitive regions is analyzed in the same manner, with Nyquist plots being presented in Fig. 5C. Compared to bulk-TiS_2, the nano-TiS_2 host material offers both smaller diffusion length and a higher surface area, impacting on the charge storage kinetics. Consequently, in the low-frequency region, an overall reduction of the solid-state diffusion-related P1 signals is observed in the DRT analysis (Fig. 5D), compared to bulk-TiS_2. The P1 resistance also further decreases in nano-TiS_2 in the pseudocapacitive compared to the battery-like region. This is significant as it indicates that even for nanosized host materials, an increased interlayer spacing is beneficial to further reduce solid-state diffusion limitations.

For mid-frequencies, processes related to interfacial ion adsorption and transport (P2, P3) in the battery-like region merge to a single signal P2* in the pseudocapacitive region. There is a drastic reduction in overall P2 and P3 intensity compared to bulk-TiS_2, in line with the increased surface area/number of insertion sites in nano-TiS_2. P4 resistance is similar in magnitude for both battery-like and pseudocapacitive intercalation regions in nano-TiS_2, and even on a comparable level to bulk-TiS_2, which is in line with the (mostly particle size- and intercalation site-independent) desolvation processes that is necessary for each intercalating ion. The results demonstrate that in nano-TiS_2, when transitioning from battery-like to pseudocapacitive

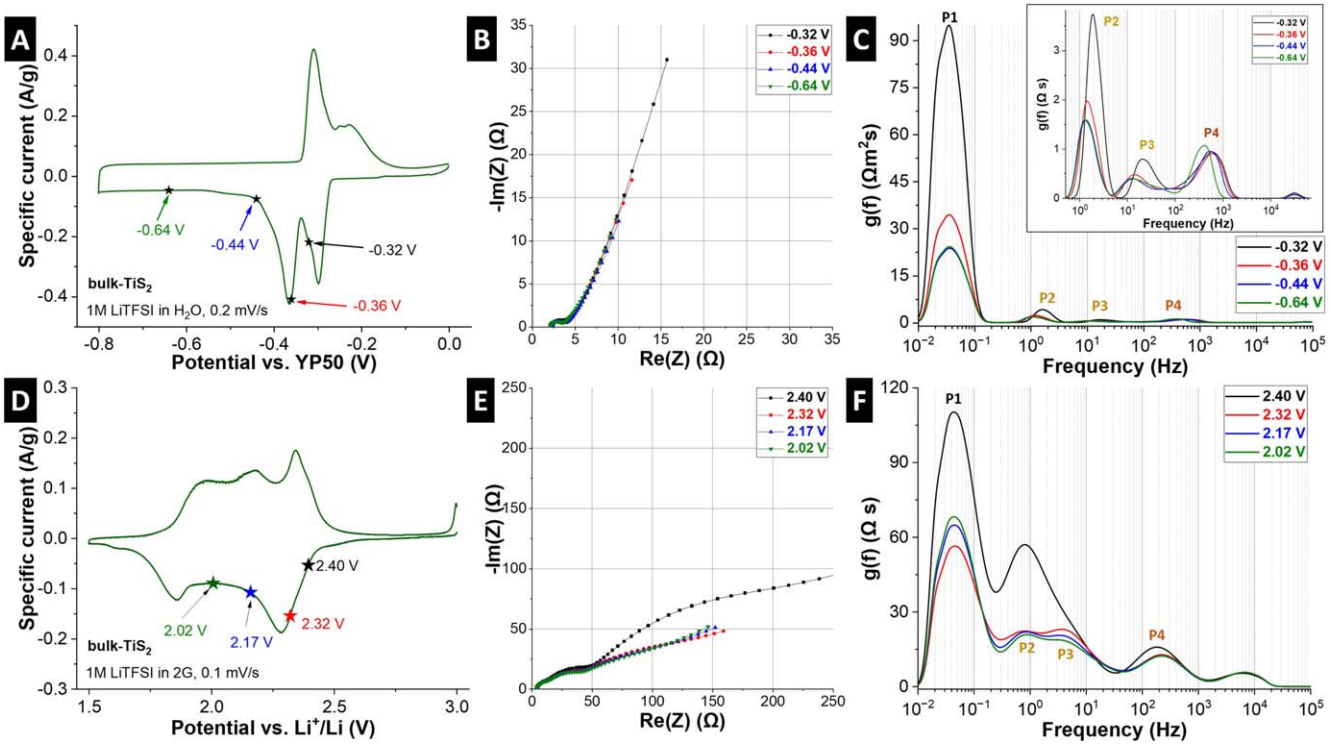

Figure 6. Investigation of Li^+ intercalation into bulk-TiS_2 from different electrolytes. (A) Cyclic voltammogram at 0.2 mV s^{-1}, (B) Nyquist plots and (C) related DRT transformations at various characteristic potentials in aqueous 1 M LiTFSI electrolyte. (D) Cyclic voltammogram at 0.2 mV s^{-1}, (E) Nyquist plots and (F) related DRT transformations at various characteristic potentials in organic 1 M LiTFSI in diglyme ("2 G") electrolyte.

Li^+ intercalation, mainly solid-state diffusion limitations are reduced, while surface adsorption/transport and desolvation limitations remain largely unaffected. The data is also replotted for a direct comparison of bulk- and nano-TiS_2 in both the battery-like (Fig. S5A) and pseudocapacitive (Fig. S5B) potential regions.

The DRT analysis reveals the large impact of the process P4 (which we assigned to the ion desolvation process) on the kinetics of the pseudocapacitive intercalation process in TiS_2. Thus, to further verify the assignment of P4 to the desolvation process, Li^+ intercalation into TiS_2 is investigated from aqueous and organic diglyme-based electrolytes due to the reported absence of the full desolvation process in these systems[37,38,54,55] (full electrochemical characterization from aqueous electrolyte in Fig. S2). Cyclic voltammograms in the two electrolytes reveal a different electrochemical signature as compared to the standard, carbonate-based LP30 electrolyte (Figs. 6A, 6D), indicative of a change of the intercalation mechanism. Impedance spectra are recorded at various characteristic potential steps over the lithiation process in aqueous (Fig. 6B) and diglyme-based electrolytes (Fig. 6E). The related DRT results (Figs. 6C, 6F) clearly indicate that in both cases, the Li^+-solvent cointercalation process is mainly limited by solid-state diffusion (P1) over the entire potential window, followed by the surface adsorption related resistances (P2/3). Notably, the desolvation-related resistance (P4) almost entirely disappears at each probed potential in aqueous electrolyte, in line with desolvation-free cointercalation mechanism. In the diglyme-based electrolyte, it represents the smallest resistance compared to P1–3 over the entire potential window, which is different from the case of bare ion intercalation in LP30 electrolyte (Figs. 5B, 5D). This point is further underlined by a direct comparison between LP30 and diglyme-based organic electrolytes is shown in Fig. S6. It should be noted that several changes of the electrochemical system (different electrolyte, current collector, reference electrode, cell type) likely prevent direct quantitative comparison of the resistances of the aqueous to the organic electrolyte systems. However, the analysis clearly shows that the cointercalation processes of Li^+ with either a H_2O- or diglyme-based solvation shell into TiS_2 show mostly solid-state diffusion limitations. Thus, the magnitude of the P4 signal may provide an experimental verification tool to probe the desolvation process during intercalation reactions.

Conclusions

In this work, we present DRT analysis of electrochemical impedance spectra to identify the kinetic limitations of the lithium intercalation reaction in the model system TiS_2. In this electrode material, studying various sub-steps of the complex, multi-step intercalation process is possible. The transition from battery-like to pseudocapacitive intercalation can be analyzed based on the potential region (or state of charge), the influence of diffusion lengths based on variable TiS_2 particle size, and the effect of solvent cointercalation based on the electrolyte solvent used. DRT allows the individual contributions of solid-state ion diffusion, interfacial ion adsorption and transport, and ion desolvation to be identified. We find that in bulk-TiS_2, upon transitioning from battery-like to pseudocapacitive intercalation, kinetic limitations of solid-state diffusion and surface adsorption are strongly reduced. For nano-TiS_2, however, transition from battery-like to pseudocapacitive intercalation is mostly reflected in reduced solid-state diffusion limitation. The resistance associated with ion desolvation remains largely unaffected by diffusion length/TiS_2 particle size and battery-like/pseudocapacitive intercalation, but can be reduced using aqueous or diglyme-based electrolytes that enable solvent cointercalation. The work provides a facile electrochemical probe for the influence of different sub-steps of the intercalation reaction in TiS_2 on the overall kinetics. In particular, various contributors to the charge transfer resistance can be distinguished. As an alternative to common voltammetry techniques like the "b-value analysis," it can be useful to gain a more detailed understanding of electrochemical intercalation reactions in other layered/2D host materials.

Acknowledgments

Y.T.M. and S.F. acknowledge funding from the German Research Foundation (DFG) in the project "NanoconEC" (project

number 513327636). S.F. acknowledges funding from the German Federal Ministry of Education and Research (BMBF) in the "NanoMatFutur" program (grant No. 03XP0423). The authors acknowledge basic funding from the Helmholtz Association.

ORCID

Yoga Trianzar Malik https://orcid.org/0000-0002-1466-9974
Patrice Simon https://orcid.org/0000-0002-0461-8268
Simon Fleischmann https://orcid.org/0000-0001-9475-3692

References

1. R. C. Massé, C. Liu, Y. Li, L. Mai, and G. Cao, "Energy storage through intercalation reactions: electrodes for rechargeable batteries." *Natl Sci. Rev.*, **4**, 26 (2017).
2. J. Y. Kim et al., "Revisiting TiS2 as a diffusion-dependent cathode with promising energy density for all-solid-state lithium secondary batteries." *Energy Storage Mater.*, **41**, 289 (2021).
3. J. B. Cook, T. C. Lin, H-S. S. Kim, A. Siordia, B. S. Dunn, and S. H. Tolbert, "Suppression of electrochemically driven phase transitions in nanostructured MoS_2 pseudocapacitors probed using operando x-ray diffraction." *ACS Nano*, **13**, 1223 (2019).
4. M. Elmanzalawy, A. Innocenti, M. Zarrabeitia, N. J. Peter, S. Passerini, V. Augustyn, and S. Fleischmann, "Mechanistic understanding of microstructure formation during synthesis of metal oxide/carbon nanocomposites." *J. Mater. Chem. A*, **11**, 17125 (2023).
5. S. Fleischmann, A. Tolosa, and V. Presser, "Design of carbon/metal oxide hybrids for electrochemical energy storage." *Chem. - A Eur. J.*, **24**, 12143 (2018).
6. H. D. Yoo et al., "Fast kinetics of magnesium monochloride cations in interlayer-expanded titanium disulfide for magnesium rechargeable batteries." *Nat. Commun.*, **8**, 339 (2017).
7. J. Choi, H. Moon, and S. Fleischmann, "Simultaneous control of crystallite size and interlayer spacing of MoS_2 to achieve pseudocapacitive lithium intercalation." *Electrochim. Acta*, **476**, 143774 (2024).
8. H. Sun et al., "Three-dimensional holey-graphene/niobia composite architectures for ultrahigh-rate energy storage." *Science*, **356**, 599 (2017).
9. H. Sun, J. Zhu, D. Baumann, L. Peng, Y. Xu, I. Shakir, Y. Huang, and X. Duan, "Hierarchical 3D electrodes for electrochemical energy storage." *Nat. Rev. Mater.*, **4**, 45.
10. M. L. Divya, Y. S. Lee, and V. Aravindan, "Solvent co-intercalation: an emerging mechanism in Li-, Na-, and K-Ion capacitors." *ACS Energy Lett.*, **6**, 4228 (2021).
11. L. Que, J. Wu, Z. Lan, Y. Xie, F. Yu, Z. Wang, J. Meng, and X. Zhang, "Potassium-based dual-ion batteries operating at −60 °C enabled by co-intercalation anode." *Adv. Mater.*, **35**, 2307592 (2023).
12. H. Guo, M. Elmanzalawy, P. Sivakumar, and S. Fleischmann, "Unifying electrolyte formulation and electrode nanoconfinement design to enable new ion—solvent cointercalation chemistries." *Energy Environ. Sci.*, **17**, 2100 (2024).
13. P. G. Bruce and M. Y. Saidi, "The mechanism of electrointercalation." *J. Electroanal. Chem.*, **322**, 93 (1992).
14. T. Okumura, T. Fukutsuka, K. Matsumoto, H. Orikasa, H. Arai, Z. Ogumi, and Y. Uchimoto, "Lithium-ion transfer reaction at the interface between partially fluorinated insertion electrodes and electrolyte solutions." *J. Phys. Chem. C*, **115**, 12990 (2011).
15. V. A. Nikitina, "Charge transfer processes in the course of metal-ion electrochemical intercalation." *Curr. Opin. Electrochem.*, **19**, 71 (2020).
16. V. Augustyn, J. Come, M. A. Lowe, J. W. Kim, P. L. Taberna, S. H. Tolbert, H. D. Abruña, P. Simon, and B. Dunn, "High-rate electrochemical energy storage through Li^+ intercalation pseudocapacitance." *Nat. Mater.*, **12**, 518 (2013).
17. C. Choi, D. S. Ashby, D. M. Butts, R. H. DeBlock, Q. Wei, J. Lau, and B. Dunn, "Achieving high energy density and high power density with pseudocapacitive materials." *Nat. Rev. Mater.*, **5**, 5.
18. S. Fleischmann, J. B. Mitchell, R. Wang, C. Zhan, D. E. Jiang, V. Presser, and V. Augustyn, "Pseudocapacitance: from fundamental understanding to high power energy storage materials." *Chem. Rev.*, **120**, 6738 (2020).
19. S. Fleischmann, Y. Zhang, X. Wang, P. T. Cummings, J. Wu, P. Simon, Y. Gogotsi, V. Presser, and V. Augustyn, "Continuous transition from double-layer to faradaic charge storage in confined electrolytes." *Nat. Energy*, **7**, 222 (2022).
20. J. Wang, J. Polleux, J. Lim, and B. Dunn, "Pseudocapacitive contributions to electrochemical energy storage in TiO_2 (Anatase) nanoparticles." *J. Phys. Chem. C*, **111**, 14925 (2007).
21. H. Shao, Z. Lin, K. Xu, P. L. Taberna, and P. Simon, "Electrochemical study of pseudocapacitive behavior of $Ti_3C_2T_x$ MXene material in aqueous electrolytes." *Energy Storage Mater.*, **18**, 456 (2019).
22. S. Pervez and M. Z. Iqbal, "Capacitive and diffusive contributions in supercapacitors and batteries: a critique of b-value and the ν–$N^{1/2}$ model." *Small*, **19**, 2305059 (2023).
23. T. S. Mathis, N. Kurra, X. Wang, D. Pinto, P. Simon, and Y. Gogotsi, "Energy storage data reporting in perspective—guidelines for interpreting the performance of electrochemical energy storage systems." *Adv. Energy Mater.*, **9**, 1902007 (2019).
24. R. R. Gaddam, L. Katzenmeier, and X. Lamprecht, "Review on physical impedance models in modern battery research." *Phys. Chem. Chem. Phys.*, **23**, 12926 (2021).
25. V. Vivier and M. E. Orazem, "Impedance analysis of electrochemical systems." *Chem. Rev.*, **122**, 11131 (2022).
26. J. S. Ko, M. B. Sassin, D. R. Rolison, and J. W. Long, "Deconvolving double-layer, pseudocapacitance, and battery-like charge-storage mechanisms in nanoscale $LiMn_2O_4$ at 3D carbon architectures." *Electrochim. Acta*, **275**, 225 (2018).
27. J. S. Ko, C-H. H. Lai, J. W. Long, D. R. Rolison, B. Dunn, and J. Nelson Weker, "Differentiating double-layer, psuedocapacitance, and battery-like mechanisms by analyzing impedance measurements in three dimensions." *ACS Appl. Mater. Interfaces*, **12**, 14071 (2020).
28. N. Kurra, S. Uzun, G. Valurouthu, and Y. Gogotsi, "Mapping (pseudo)capacitive charge storage dynamics in titanium carbide mxene electrodes in aqueous electrolytes using 3D bode analysis." *Energy Storage Mater.*, **39**, 347 (2021).
29. P-L. Taberna, P. Simon, and J. F. Fauvarque, "Electrochemical characteristics and impedance spectroscopy studies of carbon-carbon supercapacitors." *J. Electrochem. Soc.*, **150**, A292 (2003).
30. J. P. Schmidt, P. Berg, M. Schönleber, A. Weber, and E. Ivers-Tiffée, "The distribution of relaxation times as basis for generalized time-domain models for Li-Ion batteries." *J. Power Sources*, **221**, 70 (2013).
31. H. Schichlein, A. C. Müller, M. Voigts, A. Krügel, and E. Ivers-Tiffée, "Deconvolution of electrochemical impedance spectra for the identification of electrode reaction mechanisms in solid oxide fuel cells." *J. Appl. Electrochem.*, **32**, 875 (2002).
32. M. Braig and R. Zeis, "Distribution of relaxation times analysis of electrochemical hydrogen pump impedance spectra." *J. Power Sources*, **576**, 233203 (2023).
33. T. Rüther, M. Schamel, C. Plank, F. Schomburg, F. Röder, and M. A. Danzer, "Cell-to-cell variation beyond parameter analysis—identification and correlation of processes in lithium-ion batteries using a combined distribution of relaxation times analysis." *J. Power Sources*, **587**, 233677 (2023).
34. M. S. Whittingham, "Electrical energy storage and intercalation chemistry." *Science*, **192**, 1126 (1976).
35. S. Fleischmann, H. Shao, P-L. Taberna, P. Rozier, and P. Simon, "Electrochemically induced deformation determines the rate of lithium intercalation in bulk TiS_2." *ACS Energy Lett.*, **6**, 4173 (2021).
36. J. Miranda, G. Franklin, T. S. Mathis, P. L. Taberna, and P. Simon, "Unraveling the two-phase lithiation process in TiS_2 by using the combination of operando EQCM and electrochemical dilatometry techniques." *Energy Storage Mater.*, **65**, 103105 (2024).
37. L. Zhang et al., "Reversible hydration enabling high-rate aqueous Li-Ion batteries." *ACS Energy Lett.*, **9**, 959 (2024).
38. G. A. Ferrero, G. Åvall, K. A. Mazzio, Y. Son, K. Janßen, S. Risse, and P. Adelhelm, "Co-intercalation batteries (CoIBs): role of TiS_2 as electrode for storing solvated Na Ions." *Adv. Energy Mater.*, **12**, 2202377 (2022).
39. J. E. Trevey, C. R. Stoldt, and S-H. Lee, "High power nanocomposite TiS_2 cathodes for all-solid-state lithium batteries." *J. Electrochem. Soc.*, **158**, A1282 (2011).
40. D. Weingarth, M. Zeiger, N. Jäckel, M. Aslan, G. Feng, and V. Presser, "Graphitization as a universal tool to tailor the potential-dependent capacitance of carbon supercapacitors." *Adv. Energy Mater.*, **4**, 1400316 (2014).
41. M. Thommes, K. Kaneko, A. V. Neimark, J. P. Olivier, F. Rodriguez-Reinoso, J. Rouquerol, and K. S. W. Sing, "Physisorption of gases, with special reference to the evaluation of surface area and pore size distribution (IUPAC Technical Report)." *Pure Appl. Chem.*, **87**, 1051 (2015).
42. P. C. Sherrell, K. Sharda, C. Grotta, J. Ranalli, M. S. Sokolikova, F. M. Pesci, P. Palczynski, V. L. Bemmer, and C. Mattevi, "Thickness-dependent characterization of chemically exfoliated TiS2 nanosheets." *ACS Omega*, **3**, 8655 (2018).
43. H. Lindström, S. Södergren, A. Solbrand, H. Rensmo, J. Hjelm, A. Hagfeldt, and S. E. Lindquist, "Li+ Ion insertion in TiO2 (Anatase). 2. Voltammetry on nanoporous films." *J. Phys. Chem. B*, **101**, 7717 (1997).
44. T. H. Wan, M. Saccoccio, C. Chen, and F. Ciucci, "Influence of the discretization methods on the distribution of relaxation times deconvolution: implementing radial basis functions with DRTtools." *Electrochim. Acta*, **184**, 483 (2015).
45. N. Schlüter, S. Ernst, and U. Schröder, "Finding the optimal regularization parameter in distribution of relaxation times analysis." *ChemElectroChem*, **6**, 6027 (2019).
46. N. Schlüter, S. Ernst, and U. Schröder, "Direct access to the optimal regularization parameter in distribution of relaxation times analysis." *ChemElectroChem*, **7**, 3445 (2020).
47. A. Maradesa, B. Py, T. H. Wan, M. B. Effat, and F. Ciucci, "Selecting the regularization parameter in the distribution of relaxation times." *J. Electrochem. Soc.*, **170**, 030502 (2023).
48. S. R. Narayanan, D. H. Shen, S. Surampudi, A. I. Attia, and G. Halpert, "Electrochemical impedance spectroscopy of lithium-titanium disulfide rechargeable cells." *J. Electrochem. Soc.*, **140**, 1854 (1993).
49. M. D. Levi, K. Gamolsky, D. Aurbach, U. Heider, and R. Oesten, "On electrochemical impedance measurements of LixCo0.2Ni0.8O2 and LixNiO2 intercalation electrodes." *Electrochim. Acta*, **45**, 1781 (2000).
50. Y-C. Chang and H-J. Sohn, "Electrochemical impedance analysis for lithium ion intercalation into graphitized carbons." *J. Electrochem. Soc.*, **147**, 50 (2000).
51. V. A. Nikitina, S. Y. Vassiliev, and K. J. Stevenson, "Metal-ion coupled electron transfer kinetics in intercalation-based transition metal oxides." *Adv. Energy Mater.*, **10**, 1903933 (2020).
52. K. Xu, A. Von Cresce, and U. Lee, "Differentiating contributions to 'ion transfer' barrier from interphasial resistance and Li^+ desolvation at electrolyte/graphite interface." *Langmuir*, **26**, 11538 (2010).
53. A. Van Der Ven, J. C. Thomas, Q. Xu, B. Swoboda, and D. Morgan, "Nondilute diffusion from first principles: Li diffusion in Li_xTiS_2." *Phys. Rev. B - Condens. Matter Mater. Phys.*, **78**, 104306 (2008).
54. P. Srimuk, J. Lee, Ö. Budak, J. Choi, M. Chen, G. Feng, C. Prehal, and V. Presser, "In Situ tracking of partial sodium desolvation of materials with capacitive, pseudocapacitive, and battery-like charge/discharge behavior in aqueous electrolytes." *Langmuir*, **34**, 13132 (2018).
55. Y. Sun, G. Åvall, S-H. Wu, G. A. Ferrero, H. Wang, K. Mazzio, M. Bianchini, V. Baran, S. Risse, and P. Adelhelm, "Solvent co-intercalation in layered cathode active materials for sodium-Ion batteries." *Res. Sq.* (2024).